3

Flood Risk Mapping From Orbital Remote Sensing

G. Robert Brakenridge

ABSTRACT

Standardized methods for flood risk evaluation in the United States and elsewhere use extensive networks of river gauging stations and associated time series of annual flood peak discharge, many of which extend for many decades. Through these methods, risk is modeled: a flood discharge of particular calculated recurrence interval is routed through the channel and across the landscape via regulatory agency-approved hydrodynamic models. In contrast, many developing nations have a less-developed hydrological measurement infrastructure, and relatively few reliable in situ records of past flood peak discharges. The need in these regions for reliable flood hazard information can be even more critical, however. This chapter offers an alternative approach: combined analysis of (1) a 1998 to present time series of satellite passive microwave data that has recorded flood hydrographs at selected measurement sites, and (2) optical sensor imaging and mapping of the flood events, also sustained over a similar time span. These together produce an inundation record coupled to the microwave information, and allow exceedance probabilities to be assigned to the mapped inundation limits. Using this approach, standard flood probability distributions can be applied to a globally consistent observational period of record of ~20 years (1998–present). This observational flood risk information can be produced quickly for any microwave-monitored river reach and is being used to provide validation and calibration information for complementary hydrological flood risk modeling. Some nations already use satellite-based maps of any extreme flood event for floodplain regulation. Explored here, however, is a globally applicable strategy toward transforming such "mapped large flood" information into quantitative flood risk.

3.1. INTRODUCTION

Standardized methods for flood risk evaluation in the United States were developed by the United States Geological Survey over more than a century [*Klingeman*, 2005; *Wahl et al*., 1995]. They use an extensive network of river gauging stations and associated time series of annual flood peak discharge; many of these extend for 50–100 years. To meet regulatory and insurance requirements, flood risk assessments must be not only objective and scientifically defensible, but also uniformly applicable across highly variable hydrological regimes. The results are commonly subject to legal challenges as property owners contest the level of risk assigned; consistency of method is thus critical. Through these standard methods, risk is modeled: a flood discharge of particular calculated recurrence interval is routed through the channel and across the landscape via regulatory agency-approved hydrodynamic models such as HEC-RAS [*FEMA*, 2002].

Many developed nations outside the United States have similar risk evaluation methodologies. Quite commonly, a "100-year" discharge and associated floodplain are defined: this floodplain is the land area along a river where, at its margins, a 1% annual exceedance probability is calculated for inundation by floodwater (interior portions may experience much higher inundation frequencies). Thus, the probability P_e that one or more floods occurring

Dartmouth Flood Observatory CSDMS/INSTAAR, University of Colorado, Boulder, Colorado, USA

Global Flood Hazard: Applications in Modeling, Mapping, and Forecasting, Geophysical Monograph 233, First Edition.
Edited by Guy J-P. Schumann, Paul D. Bates, Heiko Apel, and Giuseppe T. Aronica.

during any period will exceed a given flood threshold can be expressed, using the binomial distribution, as

$$P_e = 1 - \left[1 - (1/T)\right]^n \quad (3.1)$$

where T is the threshold return period (e.g., 100 years) and n is the number of years in the period. For floods, the event may be measured in peak m^3/sec or height; most commonly the calculation uses a time series of annual flood peak discharges [*Flynn et al*., 2006; *Klingeman*, 2005].

In regard to this approach, many developing nations have a less-developed hydrological measurement infrastructure, and relatively few reliable in situ records of past flood peak discharges. The need for reliable flood hazard information may be even more critical, however, as agricultural and manufacturing economies expand, and population growth and migration increase settlement of floodplain lands [*Brakenridge et al*., 2016b]. In these locations, a different kind of hydrological modeling of flood hazard, generally on a relatively coarse spatial scale and without abundant stream flow records, is one approach toward addressing the need (as discussed elsewhere in this book). Such approaches do not require in situ flood measurements, but instead reconstruct the flood history from climatological data input and topography-assisted modeling.

The present chapter offers a third approach: combined analysis of (1) a 1998–present time series of satellite passive microwave data that records flood hydrographs at selected measurement sites [*Brakenridge et al*., 2012a; De *Groeve et al*., 2015a; *Van Dijk et al*., 2016] and (2) optical sensor imaging and mapping of flood events, also sustained over a similar time span.

These together produce an inundation record, which is coupled to the microwave information in order to assign exceedance probabilities to the mapped inundation limits.

Using this approach, standard flood probability distributions can be applied to a globally consistent observational period of record of nearly 20 years (1998–present). Note that a standard rule of thumb for extrapolation of flood probability distributions is 2x: if the period of annual peak flow record is 20 years, the 40-year event can be estimated. Thus, these records should allow estimation at-a-site of this discharge, and some mapped floods, if they are the largest of record, will be assigned recurrence intervals in excess of 20 years. Even a reliable 25-year floodplain (annual exceedance probability = 4%) is very useful risk information in any region where risk information is otherwise lacking, and these geospatial data can be made quickly available via the methodology and data described here.

Orbital remote sensing in the late 20th and early 21st centuries has provided a rich archive of actual flood inundation extents. For such data, see for example *Brakenridge et al*. [2016a]. Some nations already use satellite-based maps of any extreme flood event for floodplain regulation, on the simple principle that what has occurred may occur again [*de Moel et al*., 2009]. Explored here is a globally applicable strategy, however, toward transforming such mapped large flood information into quantitative flood risk. Such maps can, in turn, also be used to validate and calibrate flood risk maps created using modeling approaches.

3.2. MICROWAVE RADIOMETRY FOR MEASURING RIVER DISCHARGE

As noted, once a large flood has been mapped from space, the need is to constrain how large/how rare the mapped event is. In this regard, satellite microwave sensors provide global coverage of the Earth's land surface on a daily basis and, at certain wavelengths, without major interference from cloud cover. Gridded data products, updated in near real time, are available [*De Groeve et al*., 2015a]. The products are low in spatial resolution (best available resolution for these global coverage sensors is 8–10 km). However, using a strategy first developed for wide-area optical sensors [*Brakenridge et al*., 2003b, 2005], sensors such as AMSR-E, AMSR-2, TRMM, and GPM (Fig. 3.1) can measure river discharge changes at certain locations by monitoring the surface water area signal from individual image pixels over time.

The method is simple in concept: as rivers rise and discharge increases, water area within the single-pixel satellite gauging sites (~10 km × 10 km), as selected from a gridded global image product (Fig. 3.2), also increases [*Brakenridge et al*., 2007, 2012a; *De Groeve et al*., 2006, 2015b; *De Groeve and Riva,* 2009]. This water area change tracks river width and discharge variation in a manner analogous to how stage (river level) tracks discharge at in situ gauging stations. The relationship of flow area to discharge is via the continuity equation

$$Q = wdv \quad (3.2)$$

where Q is water discharge in m^3/sec, w is flow width, d is water depth, and v is water flow velocity (m/sec), as integrated across the flow cross section. As discharge increases, and provided the channel is not rectangular in shape, flow width increases at a cross section, and flow area increases overall within a river reach, in this case, a 10 km^2 measurement site.

Note that a ~10 km 37 GHz image pixel in these gridded products, centered over a river, is commonly "mixed"; it includes both water (low emission) and land (high emission). As the proportion of water area rises, the net emitted radiation declines. The microwave signal is thus very sensitive to flow width changes. The physical

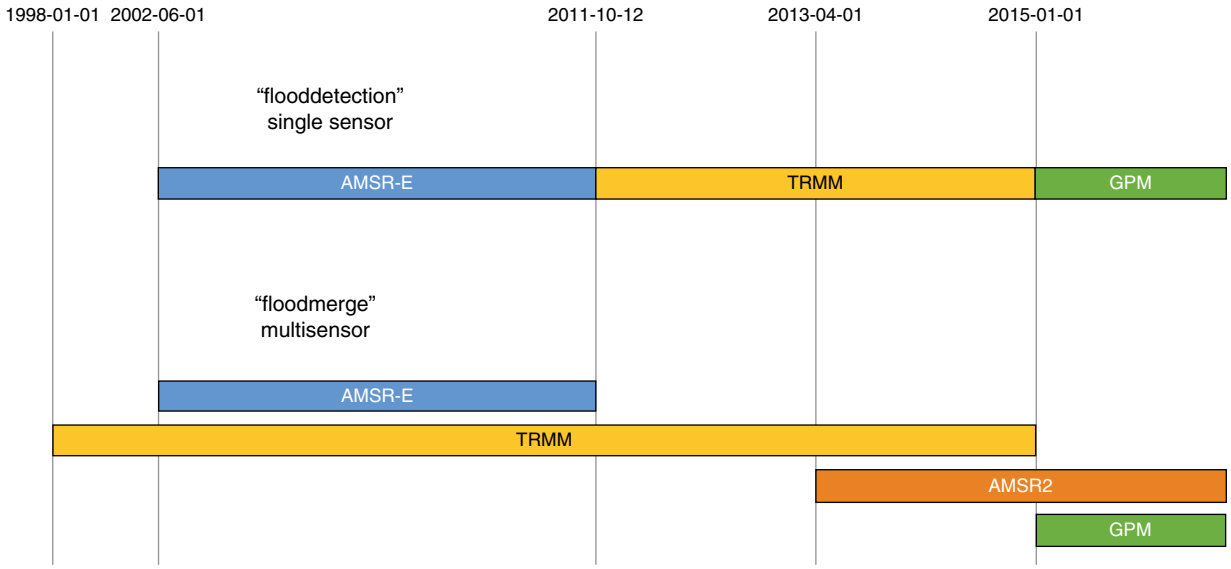

Figure 3.1 Temporal coverage, 1998 to present, of passive microwave sensors built and operated by NASA and by JAXA (Japanese Space Agency). Each satellite provides daily or near-daily imaging of the globe.

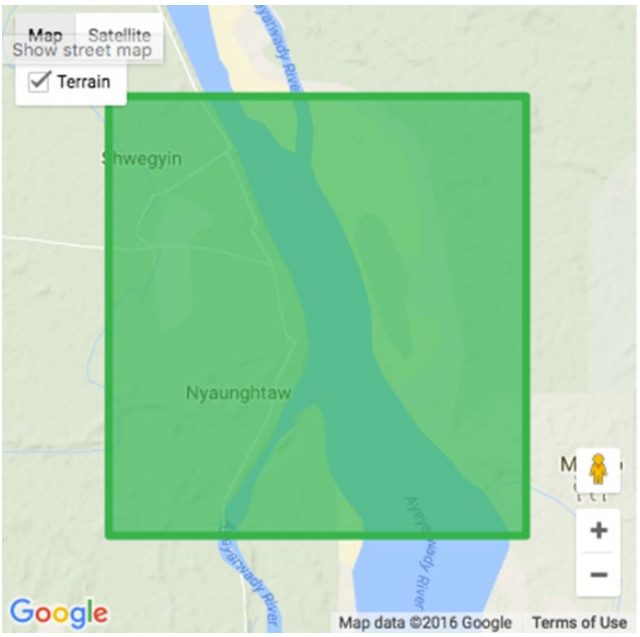

Figure 3.2 Location of Satellite Gauging Site DFO # 30 over Ayeyarwady River and its floodplain in Myanmar. The site is a single pixel selected from the JRC grid; pixel is 10 km in size and produces the daily M value. The 95th percentile of the highest (driest and warmest) values from a 9 x 9 pixel array in the surrounding area produces the background calibration C value.

mechanisms are explored elsewhere for this frequency radiation (e.g., reasons for low emission from water and much higher emission from land, *Brakenridge*, *et al.* [2007]. However, the same methodology can also use the near IR bands of optical sensors: again, water surfaces provide much lower radiance than adjoining land surfaces, but cloud cover will intermittently interfere [*Brakenridge et al.*, 2005; *Van Dijk et al.*, 2016].

As discharge along a river increases, the flow area, as seen from above, should generally increase monotonically (hysteresis effects can locally occur, however). Although in situ gauging stations instead commonly use stage, there is no a priori reason why this is a more sensitive flow monitor. If river channels are not rectangular in shape, discharge variation is expressed by both stage and width variations; and, along many rivers, width variation with flow is quite robust. Also, since a reach instead of a single cross section is monitored, the sensitivity of the flow area measurement depends on the complete suite of river/floodplain morphologic features within the reach, and including in-channel bars and low floodplain surfaces, slip-off slopes along meander bends, braided channels and islands, and floodplain oxbow lakes, which are connected to the main channel. As for in situ stations, the best satellite gauging sites thus must be carefully selected, in this case for reaches where surface area changes significantly over the full range of in-channel and flood discharges.

One implementation of satellite microwave-based flow area information for operational hydrological measurements is the River Watch processor at the Dartmouth Flood Observatory (DFO), University of Colorado (http://floodobservatory.colorado.edu/). River Watch uses the NASA/Japanese Space Agency (JAXA) Advanced Scanning Microwave Radiometer (AMSR-E) band at 36.5 GHz, the NASA/Japanese Space Agency TRMM 37 GHz channel, and 37 GHz data from the new AMSR-2

and GPM sensors. The discharge estimator (the remote sensing signal) is the ratio of the daily M, microwave emissivity from a measurement pixel centered over the river and its floodplain, and a calibrating value (C), the 95th percentile of the day's driest (brightest) emissivity within a 9 pixel × 9 pixel array surrounding the measurement pixel (Fig. 3.2). The 95th percentile excludes outliers due to sensor noise while still providing a suitable nonhydrologic background measurement. At ~37 GHz, C/M is primarily sensitive to changing surface water area within the M pixel; using the ratio removes other emission variability (e.g., from surface temperature) that affects all pixels in the area [*De Groeve et al*., 2006, 2015b; *De Groeve and Riva,* 2009].

The time series at sites within reach of TRMM (<50° latitude) begin in January 1998 (Fig. 3.1). Then AMSR-E data (merged with the TRMM information) is added when such becomes available in mid-2002. The series continues using TRMM, only, during the AMSR hiatus between AMSR-E termination and initiation of AMSR-2; Fig. 3.1) and then it adds AMSR-2 and GPM (now merging the two data streams, into 2016). The microwave record at higher latitude sites begins in mid-2002 (following launch of AMSR-E), and there is a data gap in 2012–2013 between the termination of AMSR-E and initiation of AMSR-2. The gridding algorithm that produces the global daily images is performed at the European Commission's Joint Research Centre (JRC); the original data are near–real-time swath information from each sensor provided by NASA and/or JAXA. A JRC technical document provides further information including data sources [*De Groeve et al*., 2015b].

JRC produces a daily global grid at 10 km (near the equator) pixel resolution, and publishes daily ratio data for fixed pixels within that 4000 × 2000 pixel grid. At lower latitudes, the coverage is less than daily from AMSR-E and AMSR-2: the latest River Watch version uses a forward running, 4-day mean of the daily results to avoid such data gaps. Because river discharge exhibits strong temporal autocorrelation, such averaging also provides useful smoothing and noise reduction. Also, when multiple samples for one pixel are available in 1 day, the latest sample value is used at JRC in the gridded product.

At DFO, the latest ratio data from the JRC are ingested twice each day, and the web-hosted displays and calculated discharge data for each satellite gauging site are then updated. Each site display includes two (html) online web pages: one provides plots of the results but also some tabular data (e.g., http://floodobservatory.colorado.edu/SiteDisplays/30.htm). The second presents the signal/discharge rating curve (see below) and access to the complete record of satellite-measured discharge (http://floodobservatory.colorado.edu/SiteDisplays/30data.htm).

For comparison purposes, a reference 20th percentile of the measured discharge for each day of the year is also provided and provides a useful low flow threshold.

3.3. PRODUCTION OF SIGNAL/DISCHARGE RATING CURVES

As is the case for river stage measured at in situ gauging stations, independent information is needed to translate the discharge-sensitive observable (in this case, water surface area) to the corresponding discharge value. The transformation is accomplished by an empirical rating equation that matches the signal to independent discharge information. For River Watch, the calibrating discharge values are obtained by runs of a global runoff model (WBM) [*Cohen et al*., 2011]. Five years (2003–2007) provide abundant daily model output for calibration; additional years comparing model and remote sensing could further refine and possibly extend the resulting rating curves (if larger modeled flows occur than previously). The WBM model, also using a global grid resolution of ~10 km, inputs climate and land surface variables and produces daily river discharge values for these years at each measurement site. Earlier work determined that adequate calibration information for each site's rating curve can be obtained by comparing just the monthly daily maximum, minimum, and mean values, so n = 180 for the 5-year run [*Brakenridge et al*., 2012a; *Cohen et al*., in preparation, 2013; *Cohen et al*., 2011]. Figure 3.3 provides sample results at one site as a scatter plot; Figure 3.4 illustrates the same data in time-series form. In the latter case, the signal data are first translated to discharge values using the scatter plot's rating curve in order to show the two time series on the same scale.

Without other information, it is not possible to determine which departures in a smooth monotonic relation in Figure 3.3 is from errors in the remote sensing signal and which from errors in the model. For the purpose of the flood risk assessments to be described here, however, the correlation of independent model to remote sensing further establishes that the microwave water area signal is indeed responding to discharge variation. Also, and whether or not WBM is strongly affected by model bias and is reporting consistently too-high or too-low discharge numbers, such bias will not affect the risk probabilities. Figure 3.5 provides the entire remote sensing daily time series at this satellite gauging site, and using the rating curve in Figure 3.3. Because the ratio signal is responding to surface water (and flooding) extent within the M pixel, the relative heights of the flood hydrographs shown should accurately reflect the true time series of flooding there: regardless of any model bias in the discharge calibration. This result then provides the essential information needed for flood hazard mapping: a method

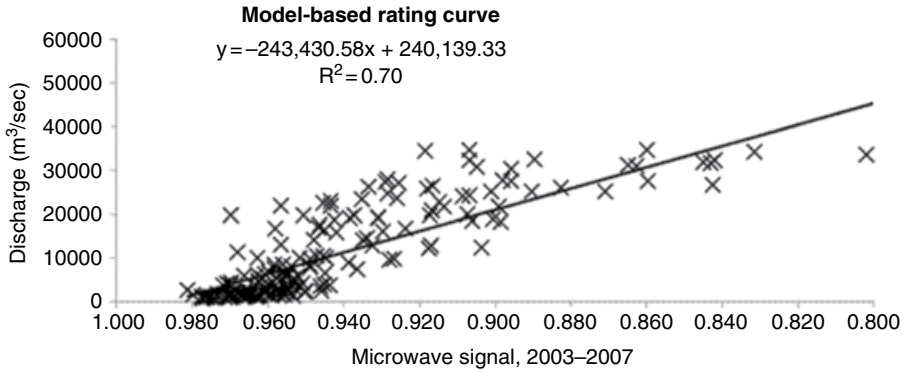

Figure 3.3 Scatter plot comparing WBM-modeled daily discharge over a 5-year period (January–December monthly daily maximum, minimum, and mean discharges) to the C/M ratio for River Watch site 30. The relationship is empirical and a better curve could be fit to these data, but a straight line is a useful first-approximation rating curve.

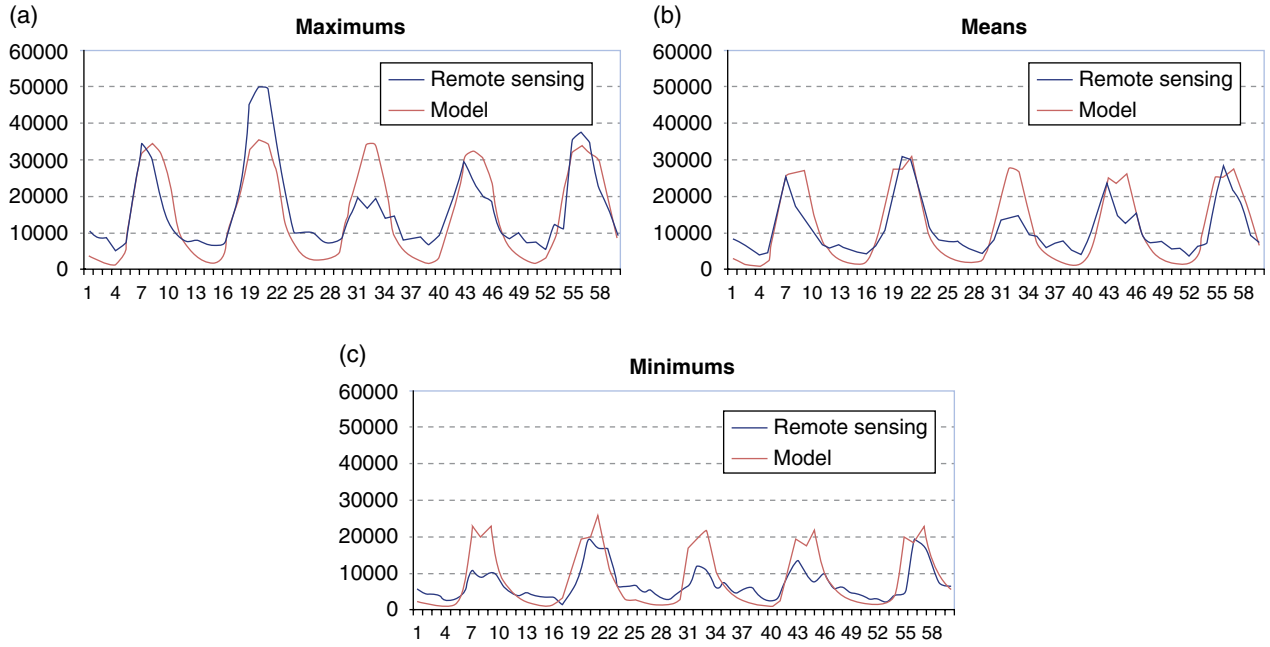

Figure 3.4 Same data as in Figure 3.3, but arranged as time series of (a) maximum, (b) mean, and (c) minimum discharge values. The red line shows the model results and the blue line is the remote sensing as transformed by the rating equation in Figure 3.3. (*See electronic version for color representation*.)

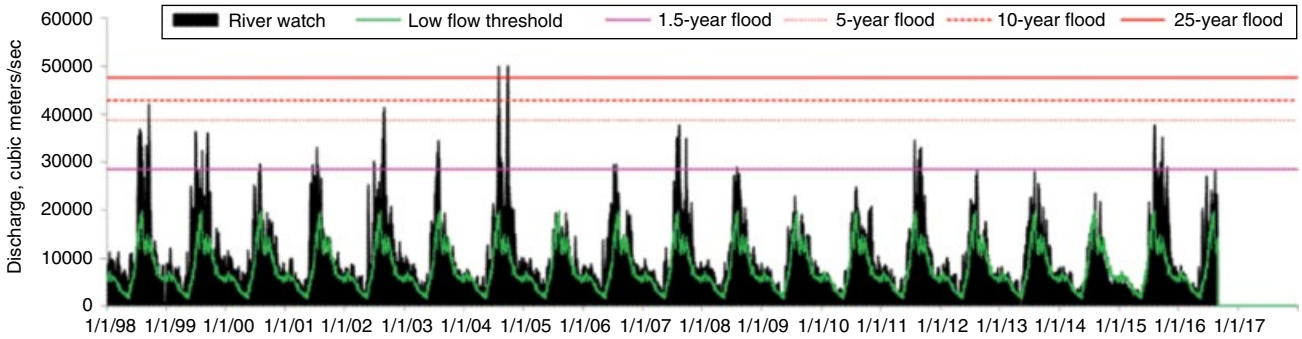

Figure 3.5 Daily (4-day forward running mean) discharge values for satellite gauging site 30 on the Ayeyarwady River. The low flow threshold (green line) is the 20% percentile discharge for each day; the flood thresholds use recurrence intervals computed using the Log Pearson III distribution and the annual maximum daily values. Major flooding in 2015 approached the calculated 5-year recurrence interval; the flood of record, in 2004, was produced by a very damaging tropical storm [*Brakenridge et al.*, 2016b]; flooding here exceeded the 25-year threshold. (*See electronic version for color representation*.)

to constrain the observed frequency/exceedance probability of an imaged flood.

There is an important factor that may change the exact return periods to be assigned to the annual flood peaks shown in Figure 3.5. That is, the straight line rating equation shown in Figure 3.3 clearly produces somewhat too high discharges for the highest water area signal values (Fig. 3.3). Adjusting the rating equation to flatten the slope would produce somewhat smaller flood peaks and also alter the corresponding return periods for the larger events. This dependency indicates the importance of developing the highest quality rating curves (the same need exists for in situ gauging stations).

3.4. ASSESSING RIVER WATCH ACCURACY

As noted, the accuracy of the satellite gauging site results depends in part on river and floodplain morphology. Other site-specific factors such as vegetation are also important [*Revilla-Romero et al*., 2014]. Using both the model and the remote sensing results, without any ground-based information, it is also possible to calculate useful statistics comparing the overall accuracy of the discharge time series results. For example, flow areas may not change very much in response to discharge along some reaches, in which case the expected signal range is small compared to the daily noise that can be induced by other factors (see below). Two descriptive statistics for a sample of sites in Myanmar along the Ayeyarwady and a major tributary (the Chindwin River) are provided as Table 3.1 to illustrate their utility and application. The "signal/model agreement" is a simple ranking and classification of the signal/model least squares regression (coefficient of determination r^2) results, as in Figure 3.3 (either for straight line fits or second order polynomials that can better match the data). Among different sites, higher r^2 indicates a stronger correlation; it is more likely that the remote sensing signal is accurately tracking river discharge variation if it is strongly correlated to modeled discharge output. These thresholds were chosen to group the r^2 values into classes: > 0.7, Excellent; 0.6–0.69, Very Good; 0.5–0.59, Good; 0.4–0.49, Fair; < 0.4, Poor.

Second, the sites vary in maximum signal range over the period of record (in Table 3.1, from a low of 0.08 to 0.20, or more than 2-fold). They also vary in the average daily signal change (from a low of 0.08 to 0.14, or nearly 2-fold). Thus, some sites may exhibit a very small total range, but significant daily variation, much of which may be noise; others a large total range and relatively small daily variation (stronger signal/noise). The ratio provides a consistent "signal strength" measure that can be similarly classified from excellent to poor. The following thresholds were chosen to group the signal/noise values into classes: > 0.8, Excellent, 0.7–0.79, Very Good, 0.6–0.69, Good, 0.47–0.59, Fair, < 0.47, Poor.

The two metrics separately provide an objective assessment of how well the remote sensing agrees with the modeling, and how strongly the signal is recording discharge variation compared with the day-to-day variation that may be mainly noise along many rivers. Known sources for noise may include (1) geolocation error (the geographic footprint of the swath image data incorporated into the gridded global product varies slightly); (2) sensor noise (the radiance measurements have finite precision); and (3) nonsurface water area effects on the ratio (so any differential environmental factors affecting the M pixel over the river and the driest pixels in the C calibration array.

Where ground gauging stations and satellite gauging sites are colocated, the remote sensing can also be directly calibrated to discharge directly via the ground information. Selected US sites (e.g., Fig. 3.6) therefore compare model-based and ground station-based rating curves, providing an assessment both of model bias and of the overall accuracy of the River Watch information. In the example shown, the river channel is meandering, but only 45 m wide; thus also demonstrating that the River Watch method is not limited to large rivers but instead requires

Table 3.1 Summary of Microwave Discharge Measurement (River Watch) Site Characteristics and Accuracy for Sites Along the Chindwin (108 and 23) and Ayeyarwady (26, 29, 30)

Site	Signal/Model Agreement	Signal Range and daily	Discharge Range	Signal/Noise	r^2
108	Very Good	0.11, 0.008	21,091 m^3/s	Good	0.66
23	Good	0.08, 0.009	25,507 m^3/s	Fair	0.57
26	Very Good	0.09, 0.013	17,242 m^3/s	Fair	0.67
29	Good	0.12, 0.014	35,891 m^3/s	Fair	0.57
30	Very Good	0.20, 0.013	35,245 m^3/s	Very good	0.70

Note: The signal range statistic records the total measured variability of the discharge-estimator signal; larger values indicate a site where the remote sensing signal is more sensitive to discharge variation. The noise statistic refers to the average signal variability on a daily basis; larger values indicate more nonhydrologic noise. The r^2 values are coefficients of least squares regression of the independent WBM modeling discharge results to the remote sensing signal (over 5 years, 2000–2010, monthly daily maximum, mean, and minimum values, n = 180).

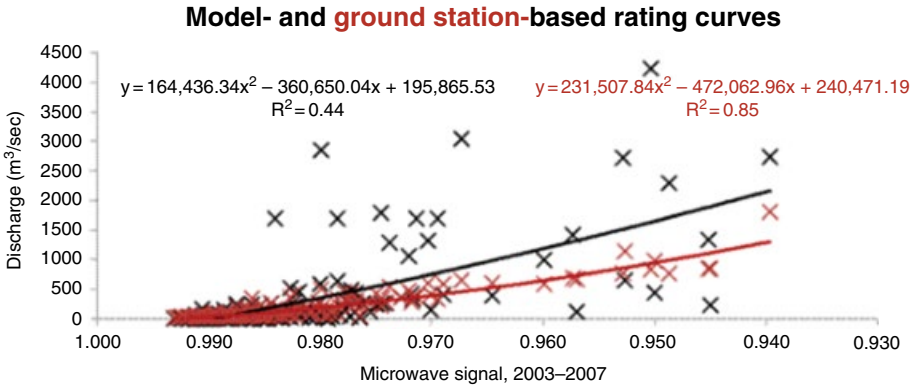

Figure 3.6 Model- and ground station-based rating curves for Trinity River, Texas, River Watch site 446 in the Dartmouth Flood Observatory/University of Colorado array. The WBM model was used to produce the black line rating curve, which is fit to widely scattered data. A colocated USGS gauging station was used to produce the red line rating curve, with much better correlation to the remote sensing. Comparison of the two curves indicates a WBM model positive discharge bias increasing with higher discharges. Also, at this location, the WBM model may perform relatively poorly because it does not incorporate upstream river control structures. (*See electronic version for color representation.*)

only floodplain/channel reaches where total surface water extent changes robustly as discharge changes.

3.5. SATELLITE GAUGING SITE SELECTION

There are several factors affecting the selection of gauging locations. It is important that the M pixel be located to avoid saturation (complete filling of the 10 km measurement pixel by water) during flood events. It is also necessary that the pixel monitors a relatively uniform stretch of river without major tributary junctions, or nearby streams, or other variable water bodies that may change in surface area without directly indicating discharge changes at the site intended. The measurement site can, however, include such river-connected features as oxbow lakes and other water-filled negative relief floodplain features [*Lewin and Ashworth*, 2014] that are connected to the river: their expansion or contraction is responsive to local river discharge changes.

Note that there may be significant time lags and hysteresis between the filling and draining of floodplains and the discharges traversing the trunk stream channel [*Brakenridge et al.*, 2007]. Consider in this regard that the microwave method is not using reach water surface area as a simple proxy for river flow width. Instead, a 10 km × 10 km parcel of floodplain and channel land with interconnected water features is recording discharge variation. The sites must be visually inspected in map form to ensure that, in each case, the flow area changes relate to the river being monitored and to evaluate the potential influence of time lags and also flow control structures along the river. Another important confounding factor is irrigated agriculture, especially rice paddies. Such farming, in either the M or the C pixel, can produce an entirely erroneous change in the signal ratio as regards discharge; instead the signal records irrigation changes.

Despite the requirement for careful evaluation of each potential river measurement site, there are at least several thousands of additional River Watch sites that could be established and beyond the ~300 now being published online (http://floodobservatory.colorado.edu/DischargeAccess.html). The microwave ratio signal information is already available for each cell of the global grid. As well, it is possible to use observed site numerical correlations to known discharge variation *en masse*: to select, via the degree of correlation, the best sites to examine further [*Van Dijk et al.*, 2016]. Through this satellite observational method, in situ gauging stations are not required to consistently evaluate flood risk along satellite-monitored river reaches and floodplains, at least for predicted recurrence intervals ranging up to approximately 40 years.

3.6. FLOOD MAPPING FROM OPTICAL SATELLITES

One useful method for mapping floods and flood hazard uses the two NASA MODIS sensors (aboard the satellites Terra and Aqua). These provide 36 optical spectral bands; most bands offer spatial resolution of 1000 or 500 m. However, two bands, in the visible and near-IR portions of the spectrum (620–670 nm, band 1, and 841–876 nm, band 2) provide spatial resolution of 250 m; band 2 in particular strongly differentiates surface water from land. Such information has been used to map the inundation extents reached by floods at many locations worldwide [*Brakenridge et al.*, 2003a; 2012b; *Policelli*, 2016] (Fig. 3.7). All of the (twice daily, global coverage)

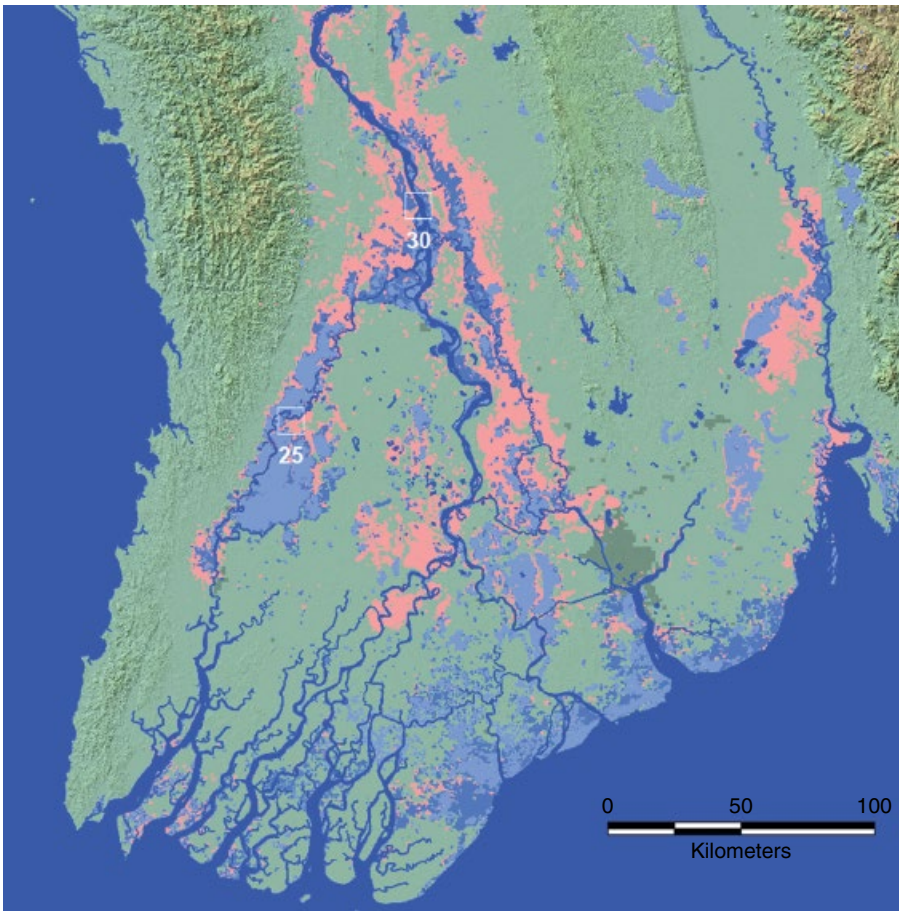

Figure 3.7 MODIS remote-sensing-produced map of major 2015 flooding in Myanmar (light red), and also the typical annual high water (2014, light blue). Recurrence intervals at the River Watch measurement sites for the 2014 "flood" are approximately 1.5 years. Dark blue is a permanent water mapped by the Shuttle Water Boundary Data (https://lta.cr.usgs.gov/srtm_water_body_dataset) from February 2000 and represents typical winter surface water extent. (*See electronic version for color representation.*)

image data since late 1999 are available in various formats in public NASA and other data archives.

As floods evolve, daily mapping of the inundation extents provides a near–real-time indication of flood severity. Flooding can be compared to previously mapped water, such as winter low flow conditions and typical annual high water (Fig. 3.7). Thus, accurate "flood" mapping does not only involve mapping maximum flood extent reached by an event, but also comparison to water extent that is typical for the same time of year. Figure 3.7 illustrates the large amount of normal annual water variability in a summer monsoon-affected region, which must first be masked before unusual flooding can be discerned. Mapping over some years can thereby provide both increasingly comprehensive flood hazard information (more probability of imaging and mapping the unusual high floods) and better information concerning what are typical and atypical high-water conditions.

3.7. REMOTE SENSING-BASED FLOOD HAZARD QUANTIFICATION

Flood inundation mapping can be coupled with either ground- or space-based river gauging to constrain the frequency of the mapped flood. Thus, using river discharge time series, standard flood frequency methods [*Flynn et al.*, 2006] can analyze the series of annual peak discharges within the period of record to evaluate flood recurrence intervals/annual exceedance probabilities for any particular event. In the United States, the Log Pearson III probability distribution is used. There are other potential issues involved in creating a risk assessment at a gauging station, particularly for large, rare events, and including the possibility to apply skewness coefficients using regional data and within the standardized Log Pearson III or other distribution functions. These techniques are well described in the literature, and provide various methods for

extending and/or extrapolating the data provided by any single river peak discharge time series.

In any case, however, the need for spatial extrapolation over a flood-prone landscape remains. A single image of a large flood event shows the inundation extent over long reaches of floodplain, and the local exceedance probability may vary significantly with location. The probability estimates obtained from a time series at a discharge time series measurement site strictly apply only to flooding at that site. This poses an interesting contrast to model-based risk mapping (see other chapters in this book): such models predict inundation from a specific recurrence interval and discharge value in a spatially continuous manner and using information about channel and floodplain morphology and flow routing equations. A flood image instead directly provides the inundation extent, without knowledge everywhere of the recurrence interval.

In flood modeling, the spatial continuity issue is implicitly addressed by interpolation. For example, the 20-year flood at site A may be calculated at 12,000 m^3/sec and that at downstream site B, 16,000 m^3/sec. At a river location midway between the two stations, and if there are no major tributary junctions, a 20-year discharge of 14,000 m^3/sec may be modeled for inundation prediction there (in grid-based modeling, this interpolation is at the grid resolution). Borrowing from this approach, if the satellite image maps a flood at both station locations, with a calculated r of 12 years at A but 18 years at B, 100 km downstream, the imaged flood limits may have, in this case, a range of r somewhere within 12 to 18 years. The risk values and map information then become even more complex, as additional floods of different return periods are mapped. Such complexity would not address the need to identify in a consistent way floodplain land areas at a particular risk of flooding.

A more practical approach is to instead divide the flooded drainage network into a series of segmented river reaches, each monitored near its midpoint by either a ground-based or space-based discharge measurement site (Figs. 3.8 and 3.9). Under this approach, the associated r is assumed to apply to the inundation extent throughout the reach, and larger or smaller floods imaged and mapped for the same reach will each also have specific recurrence intervals. In this case, no attempt is made to interpolate between river discharge measurement sites, but instead risk maps are prepared separately for each monitored river reach. A combined mapping and modeling approach, wherein the modeling provides the continuity and ability to map a particular recurrence interval flood, and the remote sensing-based mapping provides the observational validation, reach by reach, appears to be the most productive way forward for large-region mapping of flood risk [*De Groeve et al.*, 2015a].

3.8. CONCLUSION

The outlined approach couples microwave and optical remote sensing to produce quantitative flood risk maps. This chapter describes how the two can be integrated: the increasingly comprehensive global satellite map record of flood events can be matched to exceedance probabilities from microwave discharge records to produce risk maps without any in situ information. For the two examples provided, the period of satellite-microwave-observed flood discharges begins in 1998 and is now approaching 20 years. By adding the associated microwave record, the reach-level flood maps prepared from MODIS optical remote sensing show not only actual mapped floods but also the associated annual exceedance probabilities. As is the case for flood modeling products, these maps are a quantitative guide to future risk.

There is also an important additional use of such maps: for near–real-time flood inundation prediction. Unless channels and floodplains have changed since previously mapped floods (e.g., through levee construction or removal), similar flood discharges in the future along the monitored reaches should continue to produce similar inundation extents. This presents an observational rather than modeling path forward for flood inundation prediction. That is, if a particular flood hydrograph were measured, either via an in situ gauging station or the satellite microwave approach, and the resulting floodplain inundation were also observed and mapped, then the map could be used to understand what land areas will be submerged when that discharge is once again attained. A library of inundation maps could be assembled, and referred to when flooding again occurs. Note however, that flood hydrograph volume, as well as simply peak discharge and stage, may also affect maximum inundation extent, and especially over large floodplains. Flooded area is a relatively new hydrological observable that is made possible via orbital remote sensing. Productive research can now be accomplished relating different aspects of flood hydrographs to the societally and ecologically relevant variables of inundation extent and duration.

This satellite-based flood risk method is presented in outline form here, but there are complexities involved in its practical implementation and validation. For example, shortening the reach lengths and obtaining data from a denser array of discharge measurement sites would increase the accuracy and detail of risk mapping: by testing and comparing individual measurement site results. As in many other areas of work, replication of the hazard results obtained are important for the results to be trusted. Also, consider that there may be relatively large step changes between contiguous reaches in the calculated return periods for a particular mapped flood, for example, due to the influence of tributary discharges.

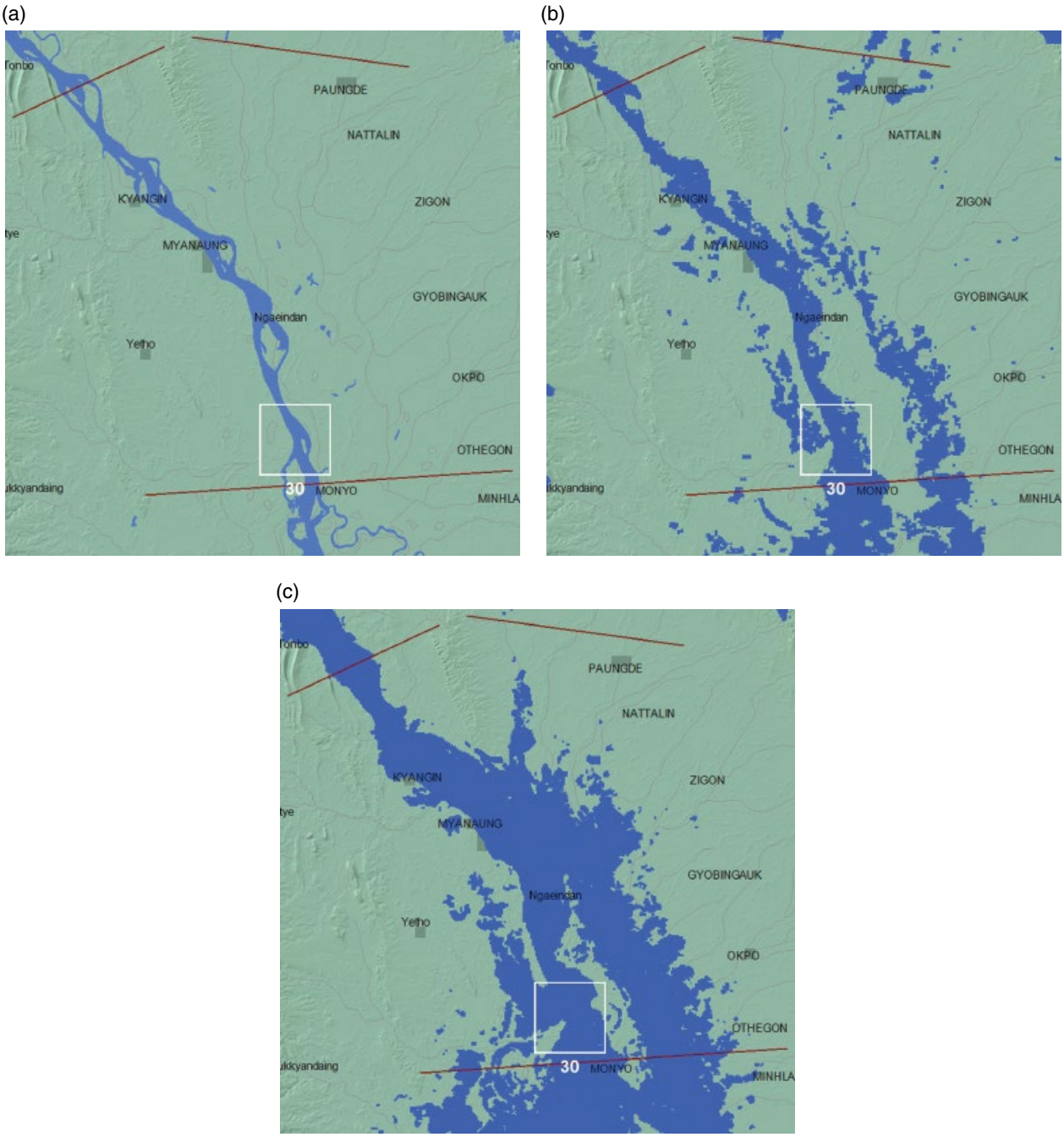

Figure 3.8 Recurrence interval and peak discharge estimates for River Watch site 30 along the lower Ayeyarwady River. The microwave measurement site is defined by the white 10 km square. Inundation for (a) a normal winter flow of 6253 m^3/sec on 11–22 February 2000; (b) observed via MODIS at 250 m spatial resolution, flooded area for a typical summer monsoonal "flood," r = 1.5 years (27,138 m^3/sec, observed 2013); and (c) observed via MODIS again, flooded area for major flooding in 2004, r = 24 years (50,579 m^3/sec. Note that during this flood, a major distributary to the east (the area is at the head of the Ayeyarwady delta) is also flooded.

This could pose a challenge in the preparation of regional maps, but also reflects the reality of the actual flood history and future risk. If regional maps are needed, another useful strategy may be to couple the described, reach-specific observational approach with regional and even global flood hazard modeling methods such as are described in other chapters in this book. For this, continuous spatial coverage via remote sensing is not needed (it is

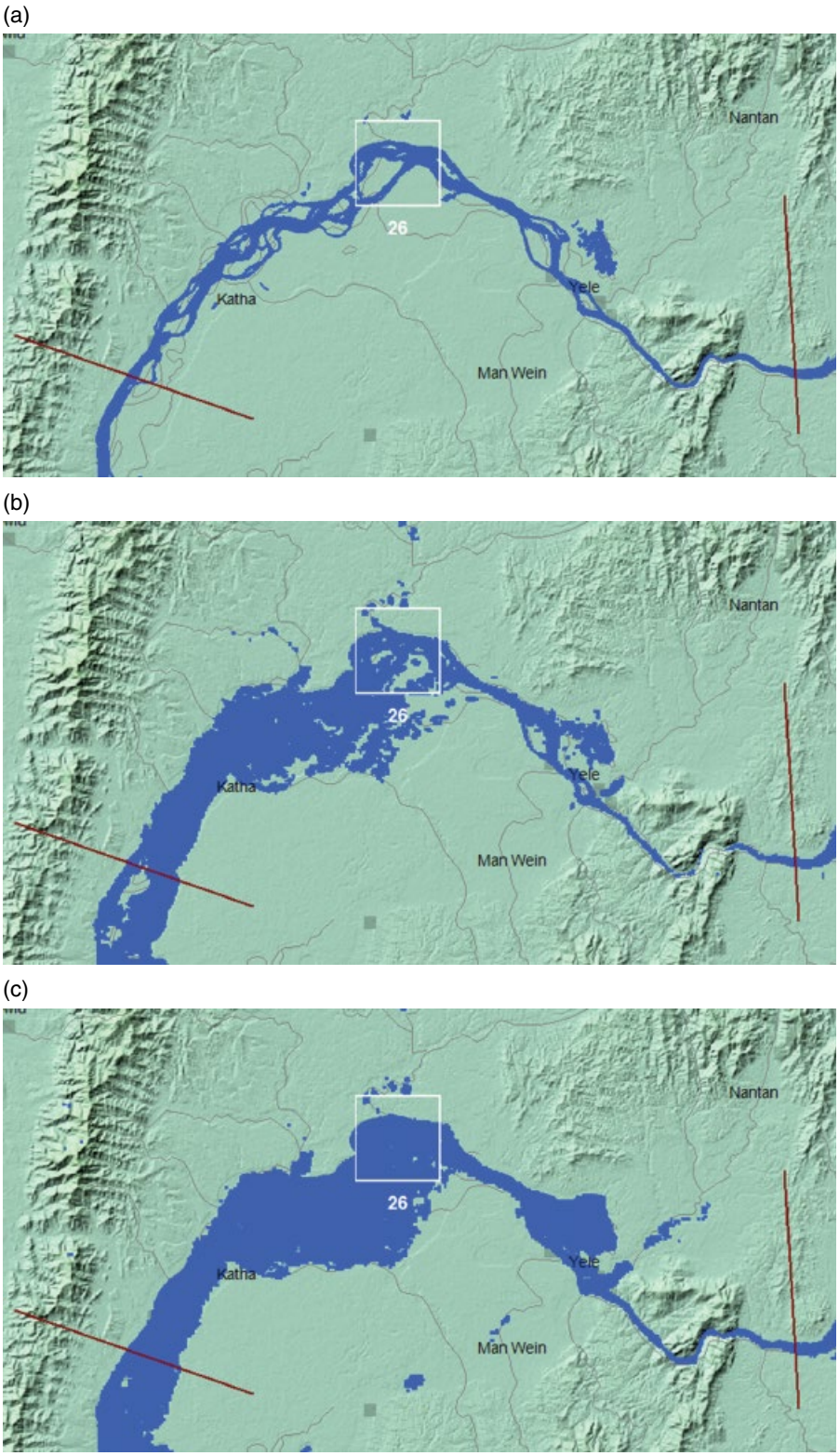

Figure 3.9 Recurrence interval and peak discharge estimates for River Watch site 26 along the upper Ayeyarwady River. Inundation for (a) a normal winter flow of ~200 m^3/sec in February 2000; (b) a typical monsoon season flood, recurrence interval of 1.1 years, ~9000 m^3/sec, in 2002; and (c) inundation during a rare flood, recurrence interval of 21 years, 18,200 m^3/sec, in 2013.

provided by the modeling). Instead, the discrete reaches where risk is characterized by remote sensing can provide critical model validation.

Finally, there is evident utility in focused attempts to image and map the very largest flood events in the period of record (e.g., the 2004 flooding in Figs. 3.5 and 3.7). Such work provides an unambiguous mapped hazard area from the most infrequent and often exceptionally damaging large events, and now their expected frequency can also be approximately constrained. Indeed, these satellite images and associated maps need to be preserved as memorials for posterity and in the same way that many communities across the globe preserve high water marks from historic extreme floods [*Davies*, 2014]. Given a changing climate, and also changes in watershed land cover and other characteristics, there is a lack of support for assuming temporal stationarity in the series of annual peak discharge [*Milly et al.*, 2008]. Yet it is only by using this assumption that probability distribution-based exceedance probabilities can be calculated. This cautions against mapping flood hazard as a static quantity. Instead, quantitative flood risk maps can be used as a starting point, and predictive models that provide information for how flood regime may change into the future should be incorporated into flood hazard mapping as well.

REFERENCES

Brakenridge, G. R., A. J. Kettner, D. Slayback, and F. Policelli (2016a), *Global Atlas of Floodplains*, Sheet 090E030N, Dartmouth Flood Observatory, University of Colorado, Boulder, CO.

Brakenridge, G. R., E. Anderson, S. V. Nghiem, and S. Chien (2005), Space-based measurement of river runof, *EOS Trans. AGU*, *86*(19), 185–188; 10.1029/2005EO190001.

Brakenridge, G. R., E. Anderson, S. V. Nghiem, S. Caquard, and T. Shabaneh (2003a), Flood warnings, flood disaster assessments, and flood hazard reduction: The roles of orbital remote sensing, *Proceedings of the 30th International Symposium on Remote Sensing of the Environment*, Honolulu, HI, 4.

Brakenridge, G. R., H. Carlos, and E. Anderson (2003b), River gaging reaches: A strategy for MODIS-based river monitoring, *Proc. SPIE 4886, Remote Sensing for Environmental Monitoring, GIS Applications, and Geology II*, 479–485; doi:10.1117/12.463105.

Brakenridge, G. R., J. P. M. Syvitski, E. Nieburh, I. Overeem, S.A. Higgins, A. J. Kettner, and L. Pradesh (2016b), Design with nature: Causation and avoidance of catastrophic flooding, Myanmar, *Earth-Science Rev.,* In review.

Brakenridge, G. R., J. P. M. Syvitski, I. Overeem, J.A. Stewart-Moore, and A. J. Kettner (2012b), Global mapping of storm surges, 2002–present and the assessment of coastal vulnerability, *Nat. Hazards*; doi: 10.1007/s11069-012-0317-z.

Brakenridge, G. R., S. Cohen, A. J. Kettner, T. De Groeve, S. V. Nghiem, J. P. M. Syvitski, and B. M. Fekete (2012a), Calibration of orbital microwave measurements of river discharge using a global hydrology model, *J. Hydrol.*; http://dx.doi.org/10.1016/j.jhydrol.2012.09.035.

Brakenridge, G. R., S. V. Nghiem, E. Anderson, and R. Mic (2007), Orbital microwave measurement of river discharge and ice status, *Water Resour. Res.*, *43*, W04405; doi:10.1029/2006WR005238).

Cohen, S., A. J. Kettner, and J. P. M. Syvitski (2011), WBMsed: A distributed global-scale riverine sediment flux model, model description and validation, *Comput. Geosci.*; doi: 10.1016/j.cageo.2011.08.011 (2011).

Davies, T. (2014), Flood and high water marks, *Flood List,* 8 August.

De Groeve, T., and P. Riva (2009), Early flood detection and mapping for humanitarian response, *Proceedings of the 6th International ISCRAM Conference*, edited by J. Landgren and S. Jul, Gothenburg, Sweden, May 2009.

De Groeve, T., G. R. Brakenridge, and S. Paris (2015a), *Global Flood Detection System Data Product Specifications*, JRC Technical Report, http://www.gdacs.org/flooddetection/Download/Technical_Note_GFDS_Data_Products_v1.pdf, Publications Office of the European Union.

De Groeve, T., Z. Kugler, and G. R. Brakenridge (2006), Near real time flood alerting for the global disaster alert and coordination system, *Proceedings ISCRAM2007*, edited by B. Van de Walle, P. Burghardt, and C.Nieuwenhuis, 33–39.

de Moel, H., J. van Alphen, and J. C. J. H. Aerts (2009), Flood maps in Europe: Methods, availability, and use, *Nat. Hazards. Earth Syst. Sci*, *9*, 289–301.

FEMA (2002), HEC-RAS procedures for HEC-2 modelers, *Floodplain Modeling Manual*, Federal Emergency Management Agency, Washington, DC.

Flynn, K. M., W. H. Kirby, and P. R. Hummel (2006), *User's Manual for Program PeakFQ*, Annual Flood-Frequency Analysis Using Bulletin 17B Guidelines, US Geological Survey, Reston, VA, 42.

Klingeman, P. (2005), Analysis techniques: Flood frequency analysis, Streamflow evaluations for watershed restoration planning and design, Oregon State University, Corvalis, OR.

Lewin, J., and P. J. Ashworth (2014), The negative relief of large river floodplains, *Earth Sci. Rev., 129*, 1–23.

Milly, P. C. D., J. Betancourt, F. Malin, R. M. Hirsch, Z. W. Kundzewicz, D. P. Lettenmaier, and R. J. Stouffer (2008), Stationarity is dead: Whither water management?, *Science*, *319*, 573–574.

Policelli, F. (2016), The NASA global flood mapping system, in *Remote Sensing of Hydrologic Extremes*, edited by V. Lakshmi, Springer-Verlag.

Revilla-Romero, B., J. Thielen, P. Salamon, T. De Groeve, and G. R. Brakenridge, (2014), Evaluation of the satellite-based Global Flood Detection System for measuring river discharge: Influence of local factors, *Hydrol. Earth Syst. Sci.*, *18*, 4467–4484.

Van Dijk, A. I. J. M., G. R. Brakenridge, A. J. Kettner, J. E. Beck, and T. De Groeve (2016), River gauging at global scale using optical and passive microwave remote sensing, *Water Resour. Res.*, *52*, 6404–6418.

Wahl, K. L., W. O. Thomas, and R. M. U. Hirsch (1995), *Stream-Gaging Program of the U.S. Geological Survey*, USGS Circular 1123, U.S. Geological Survey.